Journal of Catalysis **192,** 48–53 (2000)
doi:10.1006/jcat.2000.2823, available online at http://www.idealibrary.com on IDEAL®

Occurrence and Mechanism of Formation of CeOCl in Pd/CeO_2 Catalysts

Leszek Kępiński[1] and Janina Okal

Institute of Low Temperature and Structure Research, Polish Academy of Sciences, P.O. Box 1410, 50-950, Wrocław, Poland

Received July 30, 1999; revised January 10, 2000; accepted January 10, 2000

The formation of the CeOCl phase in a $Pd(Cl)/CeO_2$ catalyst during reduction in hydrogen was studied by HRTEM, XRD, and low-temperature N_2 adsorption (BET). The results indicate that CeOCl crystallites nucleate at (110) faces of CeO_2 crystals at $T \leq 300$°C and then grow by coalescence of existing nuclei and attachment of Ce–O–Cl species continuously formed at the ceria surface. Lateral growth of CeOCl results in rapid decline of the BET surface of the catalyst between 300 and 500°C due to the "enwrapping" of the grains of the catalyst. The mechanism of an ordered CeOCl–CeO_2 transformation in an oxidizing atmosphere is proposed. © 2000 Academic Press

Key Words: **Pd/CeO_2 catalyst; effect of chlorine; CeOCl formation; BET; HRTEM.**

Heterogeneous metal catalysts containing a lanthanide oxide as a support or as an additive are widely used due to their unique oxygen storage properties. When such catalysts are prepared from chlorine-containing metal precursors, chlorine is very strongly bound to the *Ln* oxide, so that standard catalyst pretreatment (calcination and reduction at 400°C) (1–4) and even reduction above 700°C (5–8) leave most of the chlorine in the catalyst. During reduction above 300°C, chlorine forms stable *Ln*OCl phases with tetragonal (PbFCl type) structure with *Ln* oxides (1, 2, 5–8). Though such compounds are well known, their presence is sometimes overlooked in catalytic studies. In a recent paper on Pd/Al_2O_3–La_2O_3, Bogdanchikova *et al.* (9) deduced from XRD the formation upon reduction of a "new crystalline phase," which is in fact LaOCl (10). Fan and Fujimoto (11) interpreted their XRD spectrum of Pd/CeO_2 reduced at 500°C misleadingly, considering the occurrence of CeOCl peaks (cf. (8)) as evidence for the formation of Ce_2O_3 oxide, which is improbable at such a low temperature.

The aim of this article is to draw attention to the problem of the frequent formation and possible effects of *Ln*OCl phases in *Me*/*Ln* oxide catalysts prepared from chlorine-containing precursors. We will also present a new, consistent model of growth of such phases based on experimental results obtained for a $Pd(Cl)/CeO_2$ catalyst. The evolution of the structure of Pd and of its interaction with ceria support has been described in a previous paper (5) and will not be considered here.

The catalyst studied was the same as that in (5). It was prepared by evaporation and drying (at 80°C overnight) of a mixture of suitable amounts of an aqueous solution of $PdCl_2$ and a 20 wt% colloidal dispersion of CeO_2 in dilute acetic acid (Aldrich). The catalyst contained 9 wt% Pd and 8 wt% Cl, and even prolonged reduction (20 h) at 700°C did not change these values (5). The structure of the catalyst after reduction in H_2 at 150–700°C was studied by HRTEM (Philips CM 20 SuperTwin microscope), XRD (Stoe powder diffractometer), and BET surface area measurement (N_2 adsorption at the LN_2 temperature). Following reduction, the samples were cooled to room temperature in H_2 flow and then were slowly exposed to air. It has been established that contrary to $Pd(N)/CeO_2$ samples prepared from Pd nitrate, the samples prepared from Pd chloride were relatively stable (no changes in the XRD patterns were detected after 1 h of exposure to air (5)). As a reference we also studied the bare CeO_2 support prepared by evaporation and drying of the colloidal dispersion of CeO_2 used for preparation of the catalyst. Specimens for TEM were obtained by dipping a microscope grid covered with perforated carbon into freshly reduced samples. The grid was then immediately transferred into the microscope. The most important results are collected in Table 1. The L_{BET} values were calculated from the S_{BET} values according to the formula $L_{BET}\,[\mathrm{nm}] = 6000/(\rho\,[\mathrm{g/cm^3}] \times S_{BET}\,[\mathrm{m^2/g}])$ with $\rho_{CeO2} = 7.3$ g/cm^3. The L_{XRD} values were established from the broadening of the peaks in the XRD pattern (with the Scherrer formula), and the L_{TEM} values were estimated from the HRTEM micrographs.

Figure 1 shows HRTEM micrographs of the $Pd(Cl)/CeO_2$ sample reduced at 150°C (a), 300°C (b), 500°C (c), and 700°C (d) for 20 h. At 150°C (Fig. 1a) only CeO_2 crystallites in the size range of 4–6 nm, often in the [110] orientation (as determined by the digital FFT (fast Fourier transform) method—programme Crisp (12)), exposing various crystal faces, are visible. No lines other than those of cubic CeO_2 were present in the SAED and XRD patterns. At 300°C (Fig. 1b) new features in the size range of 5–15 nm, exhibiting parallel ~0.7-nm lattice fringes originating from CeOCl (001) crystal planes, are clearly seen in

[1] Corresponding author. Fax: (48-71) 344 10 29. E-mail: kepinski@int.pan.wroc.pl.

0021-9517/00 $35.00

TABLE 1

Characteristics of Pd(Cl)/CeO_2 and CeO_2 Samples Reduced at Various Temperatures

			CeO_2			CeOCl	
Sample	S_{BET} (m^2/g)	L_{BET} (nm)	L_{XRD} (nm)	L_{TEM} (nm)	a_{XRD} (nm)	L_{XRD} (nm)	L_{TEM} (nm)
			Pd/CeO_2				
H_2, 150°C	102	8	5.1	4–6	0.545	n.o.[a]	n.o.
H_2, 300°C	81	10	5.0	4–6	0.546	n.o.	5–15
H_2, 400°C	n.m.[a]	—	5.6	5–8	0.544	19	10–20
H_2, 500°C	39	21	6.6	5–10	0.545	28	10–40
H_2, 600°C	13	63	6.8	8–20	0.547	44	20–60
H_2, 700°C	8	103	20.0	10–30	0.557	42	20–90
			CeO_2				
H_2, 150°C	136	6	6.1				
H_2, 300°C	133	6.2	n.m.				
H_2, 400°C	94	8.7	7.3				
H_2, 500°C	66	12.4	9.9				
H_2, 600°C	13	63.2	n.m.				
H_2, 700°C	4	205	19.8				

[a] n.m. = not measured; n.o. = not observed.

addition to CeO_2 crystallites. The presence of CeOCl crystallites was also undoubtedly confirmed by SAED (5). Since no CeOCl peaks could be detected in the XRD pattern of this sample (5), despite a quite large projected mean size of the crystallites observed by HRTEM and although fringes of the other crystallites lying "below" the CeOCl crystallites are clearly seen, we expect that the latter must be flat, quasi-two-dimensional objects. An interesting situation is seen in the regions marked A and B in Fig. 1b, where ~0.7-nm fringes (formed by doubling CeO_2 (111) fringes) begin at the CeO_2 crystallites and extend far beyond the crystallites. The FFT pattern of the CeO_2 crystallite B (on which CeOCl crystallite nucleates) (Fig. 2) indicates an orientation close to [110] and an expanded and slightly deformed lattice: $d_{(1\text{-}1\text{-}1)} = 0.337$ nm, $d_{(1\text{-}11)} = 0.334$ nm, and an angle between these planes of 73.4°. Alignment of the CeOCl (001) and CeO_2 (1-11) planes is also seen. For comparison we analysed FFT patterns of other CeO_2 crystallites in [110] orientation in Fig. 1a and Fig. 1b (crystallites not connected with CeOCl, e.g., crystallite C). The measured values of $d_{(111)} = 0.315$–0.326 nm and an angle of

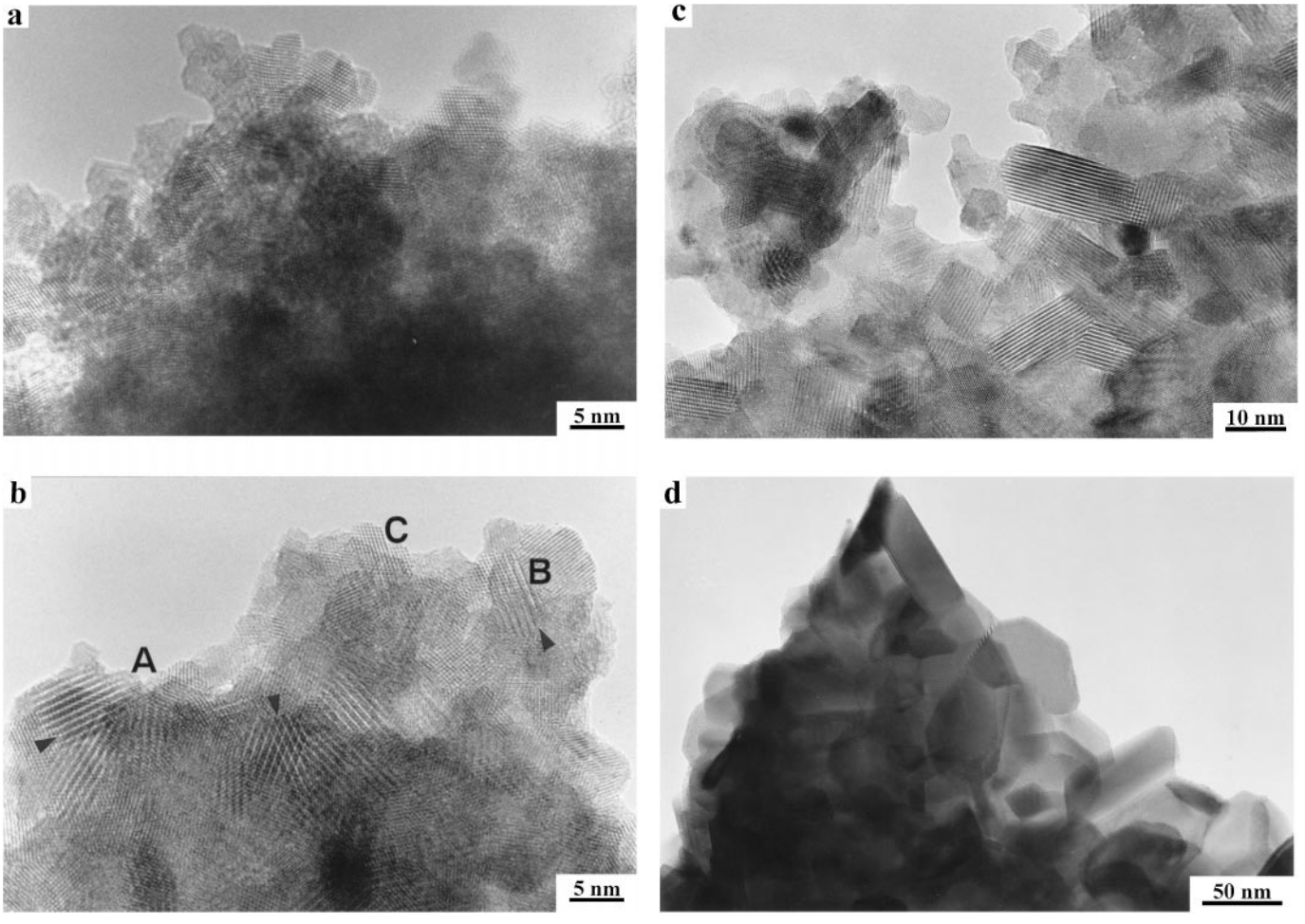

FIG. 1. HRTEM micrographs of the Pd(Cl)/CeO_2 catalyst reduced at 150°C (a), 300°C (b), 500°C (c), and 700°C (d) for 20 h. CeOCl (001) fringes (~0.7 nm) are marked in (b).

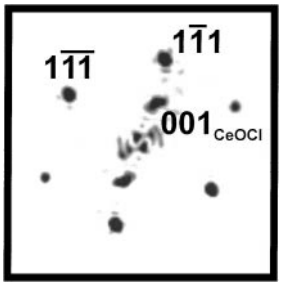

FIG. 2. FFT pattern of the CeO_2 crystallite in [110] orientation in contact with CeOCl (marked B in Fig. 1b).

70°–72° were significantly smaller and closer to those of the "ideal" CeO_2 lattice. It appears therefore that some distortion of the CeO_2 lattice may accompany CeOCl nucleation. At 500°C (Fig. 1c) large, three-dimensional CeOCl crystallites of sizes up to 40 nm are visible, together with small (~6 nm) CeO_2 crystallites. At 700°C (Fig. 1d) rapid sintering of CeO_2 and further growth of CeOCl crystals are observed (5). The image magnification in Fig. 1d is decreased to present the overall structure of the sample. As a result, no lattice fringes can be resolved. Fringes visible in Fig. 1d are actually moire fringes originating from double diffraction of superimposed crystallites. In the SAED pattern of this sample mostly strong, spotty lines of CeOCl were seen (5).

MECHANISM OF CeOCl FORMATION

Results presented in Table 1 and in Figs. 1 and 2 allow us to propose the following model of CeOCl formation in the systems containing CeO_2 and chlorine that are subjected to reduction in H_2.

Experiments with high surface CeO_2 doped with noble metals showed that hydrogen treatment at 150°C results in oxygen loss corresponding to complete surface reduction of ceria (6, 13, 14). Cl^- ions, if present, are incorporated into the oxygen vacancies at the CeO_2 surface (6):

$$(O^{2-}Ce^{4+}O^{2-})(O^{2-}Ce^{4+}O^{2-}) + 2H^+Cl^- + H_2$$
$$\Rightarrow (O^{2-}Ce^{3+}Cl^-)(O^{2-}Ce^{3+}Cl^-) + 2H_2O.$$

In this process, at maximum 50% of the surface O^{2-} ions can be replaced by Cl^- and a surface CeOCl phase is formed. Theoretical calculations show that the energy of oxygen vacancy formation at the CeO_2 surface varies strongly with the surface structure and is three times lower on (110) than on (111), where it is equal to the energy for the vacancy formation in the bulk (15, 16). Since bulk reduction of CeO_2 does not occur below 250°C for Me/CeO_2 or below 600°C for bare CeO_2 (6, 17), we have to assume that the high surface CeO_2 used as the catalytic support must expose a significant fraction of "easily" reduced, e.g., (110), faces. If every second row of O^{2-} ions in the (110) surface (marked gray in Fig. 3) is replaced by Cl^- and all ions are slightly rearranged (the Cl^- radius (0.181 nm) is much larger than that of O^{2-} (0.135 nm)), then we obtain the CeOCl (010) surface (Fig. 3).

Between 150 and 300°C CeOCl crystallites discernible by HRTEM begin to grow. We assume that (110)-type CeO_2 surface planes play an important role as nucleation centers for CeOCl crystal growth. In addition to the crystallographic match mentioned previously these surfaces exhibit a strong tendency to segregation of oxygen vacancies formed inside the bulk of CeO_2 (15, 16), allowing Cl^- incorporation into the subsurface layer. Extended, quasi-two-dimensional CeOCl crystallites observed in Fig. 1b probably grow by coalescence of the closely spaced nuclei and capture of some Ce–O–Cl species migrating over the surface. The process accelerates at higher temperatures so that three-dimensional CeOCl crystallites (detected by XRD) are formed at or above 400°C (5) and continues until all Cl^- ions are consumed. The growing crystals cover the neighbouring CeO_2 crystallites, blocking some of the existing micropores. As a result the S_{BET} of the catalyst, contrary to that of the bare support, declines already at low temperatures (Fig. 4). Moreover, there is a large discrepancy for the catalyst, between the mean crystallite sizes of CeO_2 as determined from BET and XRD, while such an effect is not present for the support (Table 1). We believe that the sudden decline in the activity of the Pd(Cl)/CeO_2 catalyst in benzene hydrogenation observed after reduction at 400°C (and not occurring for the catalyst prepared from Pd nitrate) reported in our previous work (5) can be explained by this effect.

Above 500°C there is a rapid decline of the BET surface area for both Pd(Cl)/CeO_2 and CeO_2 samples caused by enhanced sintering of CeO_2 induced by the formation

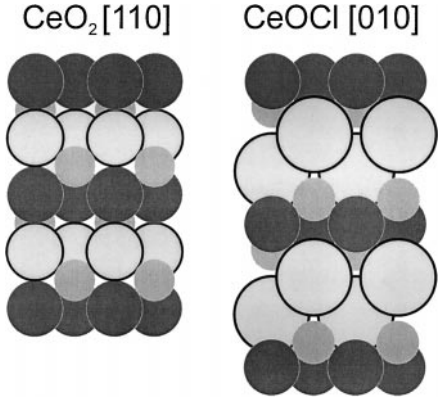

FIG. 3. Structure relation between CeO_2 (110) and CeOCl (010) surfaces. Oxygen ions, medium black and gray balls; Ce ions, small balls; Cl ions, large balls. Replacement of the gray O^{2-} ions in CeO_2 with Cl^- gives a CeOCl (010) plane.

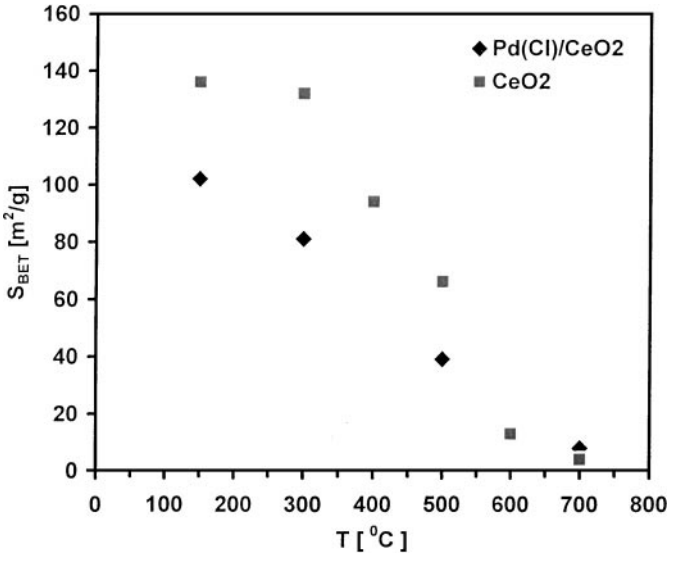

FIG. 4. Change of S_{BET} with the temperature of reduction for the Pd(Cl)/CeO_2 catalyst and CeO_2 support.

of oxygen vacancies in the bulk (15, 17). Simultaneously, further growth of CeOCl crystallites is also observed. At 700°C, additionally, as revealed by XRD, the whole amount of CeO_2 is converted into an oxygen-deficient CeO_x with a lattice parameter of 0.557 nm (Table 1). The CeO_x formed in chlorine-free samples reoxidizes rapidly when exposed to air at room temperature, but is relatively stable in the systems containing chlorine (5). This observation can also be explained by the proposed model, assuming enwrapping of ceria crystallites within grains of the catalyst by the CeOCl phase formed at the grain surface.

As shown above, the CeOCl crystallites are always at least twice as big as the CeO_2 crystallites in the same sample. For the Pd/CeO_2/SiO_2 sample (1 wt% Pd, prepared from $PdCl_2$ precursor) reduced at 600°C (18) we even observed ribbon-like CeOCl crystallites up to 100 nm long coexisting with small (∼6-nm) CeO_2 crystallites. Since the volume increase connected with the CeO_2 (cubic) ⇒ CeOCl (tetragonal) structure transformation is 44% (8), which corresponds to only an ∼15% increase in size, the CeOCl cannot grow by a mechanism proposed by Fajardie *et al.* (6), which assumes direct replacement of oxygen ions in the CeO_2 structure with Cl^-. Such a mechanism is also unrealistic due to the large difference between the ionic radii of O^{2-} (0.135 nm) and Cl^- (0.181 nm). Instead, we propose that CeOCl crystals grow by some kind of mass transport from CeO_2 crystallites (possibly mediated by chlorine) and coalescence of neighbouring crystallites.

The presence of a noble metal is not necessary for CeOCl formation. However, it facilitates the surface reduction of CeO_2 at low temperatures (by hydrogen spillover) and thus lowers the temperature of CeOCl formation (5, 6).

STABILITY OF CeOCl PHASE

There is evidence that in the *Me*(Cl)/CeO_2 system the CeOCl phase is stable in a H_2 atmosphere up to 700°C (5, 7), or even 800°C (6). The situation is, however, more complex in a Pd/CeO_2/SiO_2 sample, where CeOCl crystallites become unstable at 700°C, probably being transformed into cerium silicate (18).

In an oxidizing atmosphere CeOCl decomposes slowly at room temperature with possibly only a partial loss of chlorine (5, 6). Kili *et al.* (4) showed by XPS that exposure of the reduced Pd(Cl)/CeO_2/Al_2O_3 catalyst containing Pd^0 and Ce^{3+} ions to air resulted in partial chlorination of Pd and oxidation of Ce^{3+} to Ce^{4+}. Subsequent reduction in H_2 restored the CeOCl phase (4, 6). Here, we present evidence that in air tetragonal CeOCl crystallites transform directly into cubic CeO_2. Figure 5a shows a HRTEM image of a CeOCl crystal in the [010] orientation in the Pd(Cl)/CeO_2 sample reduced at 600°C and exposed to air for 4 h. The crystal has a rectangular outline with longer sides parallel to the CeOCl (001) crystal planes. The shorter edge of the crystal clearly shows a serious distortion of the structure. In Fig. 5b FFT patterns and filtered images obtained from three different places, A, B, and C, of the crystal are presented. The deviation from the *mm* symmetry in the FFT patterns, especially for region B, indicates that the crystal is tilted from the zone axis. From the FFT pattern we established that the image was taken at the Scherzer defocus, with low astigmatism, and that the tilt axis formed a 40° angle with the c^* (001) reciprocal vector. To properly identify the crystal structure, we compared the experimental (filtered) images with the images calculated for an ideal CeOCl crystal in the [010] orientation. The calculations were performed for a crystal thickness between 0.4 and 12 nm, at the Scherzer defocus, for a crystal tilt between 17.5 and 70 mrad, and for tilt axis angles of 30°, 40°, and 50°. Since the variation of the tilt axis angle did not change the images qualitatively, only the results for 40° are presented in Fig. 5b. The calculations have been performed by a multislice method with the HREM module of the Cerius^2 software package (Molecular Simulations Inc.). Additionally in Fig. 5b are shown FFT patterns calculated from the simulated images (representative patterns for the 30-mrad crystal tilt are only presented). The atomic structure at the edge (A) does not fit that of CeOCl and in fact corresponds well with cubic CeO_2 in the [110] orientation. The structure in the bulk (C) fits well with the structure of CeOCl in the [010] orientation. The region close to the edge (B) exhibits periodicities characteristic of CeOCl (0.41 × 0.68 nm), but its symmetry is inappropriate (presence of strong symmetry-forbidden (100) spots in the FFT pattern of the experimental image). Though weak, forbidden (100) CeOCl reflections appear in the FFT pattern of the calculated images due to the crystal tilt, the experimental image differs qualitatively from the

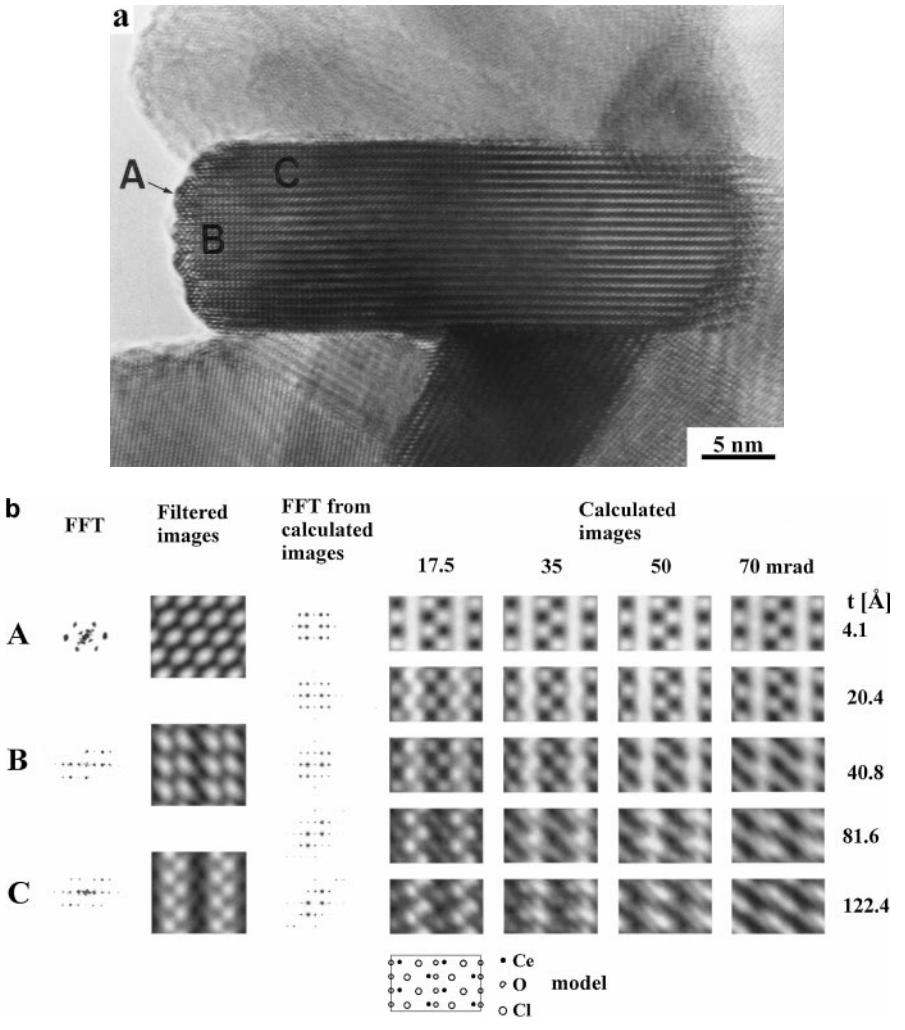

FIG. 5. An ordered CeOCl ⇒ CeO_2 transformation in an oxidizing atmosphere. HRTEM image (a) and its interpretation (b).

calculated images. We assume therefore that these deviations from the proper symmetry may be caused by a deficiency of Cl^- ions and/or their replacement with O^{2-} ions. From Fig. 5 the following crystallographic relationships between CeOCl and CeO_2 structures appear:

$$CeOCl\,[010] \parallel CeO_2\,[110] \quad \text{and} \quad CeOCl\,[001] \parallel CeO_2\,[001].$$

It appears from Fig. 5 that in an oxidizing atmosphere the CeOCl (100) face is unstable and undergoes a reconstruction so that CeO_2 (111) planes grow parallel to the CeOCl (101) surface. Cl^- ions replaced by oxygen remain at the surface of the catalyst, possibly in the vicinity of the metal particles (4). On the other hand, CeO_2 growing at the surface of CeOCl crystals protects them against further oxidation so that a significant amount of the CeOCl phase remains in Pd(Cl)/CeO_2 samples exposed to air for a few months (5, 6).

ACKNOWLEDGMENTS

The authors thank Dr. M. Wołcyrz and Dr. J. Janczak for performing the XRD measurements and A. Cielecka and Z. Mazurkiewicz for skillful technical assistance. Multislice calculations of HRTEM images and diffraction patterns were performed on the computers of the Wrocław Center of Networking and Supercomputing.

REFERENCES

1. LeNormand, F., Barrault, J., Breault, R., Hilaire,, L., Kili, K., Maire, G., and Kiennemann, A., *J. Phys. Chem.* **92**, 2561 (1988).
2. LeNormand, F., Barrault, J., Breault, R., Hilaire, L., and Kiennemann, A., *J. Phys. Chem.* **95**, 295 (1991).
3. Kondarides, D. I., and Verykios, X. E., *J. Catal.* **174**, 52 (1998).
4. Kili, K., Hilaire, L., and LeNormand, F., *Phys. Chem. Chem. Phys.* **1**, 1623 (1999).
5. Kępiński, L., Wołcyrz, M., and Okal, J., *J. Chem. Soc. Faraday Trans.* **91**, 507 (1995).
6. Fajardie, F., Tempere, J. F., Manoli, J. M., Djega-Mariadassou, G., and Blanchard, G., *J. Chem. Soc. Faraday Trans.* **94**, 3727 (1998).
7. Bernal, S., Botana, F. J., Calvino, J. J., Cifredo, G. A., and Perez-Omil, J. A., *Inst. Phys. Conf. Ser.* **138**, 485 (1993).

8. Wołcyrz, M., and Kępiński, L., *J. Solid State Chem*. **99**, 409 (1992).
9. Bogdanchikova, N. E., Fuentes, S., Avalos-Borja, M., Farias, M. H., Boronin, A., and Diaz, G., *Appl. Catal. B* **17**, 221 (1998).
10. Powder Diffraction File Nr. 34-1494.
11. Fan, L., and Fujimoto, K., *J. Catal.* **150**, 217 (1994).
12. Hovmöller, S., *Ultramicroscopy* **41**, 121 (1992).
13. Perrichon, V., Laachir, A., Bergeret, G., Frety, R., Tournayan, L., and Touret, O., *J. Chem. Soc. Faraday Trans.* **90**, 773 (1994).
14. Bernal, S., Calvino, J. J., Cifredo, G. A., Gatica, J. M., Perez-Omil, J. A., and Pintado, J. M., *J. Chem. Soc. Faraday Trans.* **89**, 3499 (1993).
15. Balducci, G., Kaspar, J., Fornasiero, P., Graziani, M., and Islam, M. S., *J. Phys. Chem. B* **102**, 557 (1998).
16. Conesa, J. C., *Surf. Sci.* **339**, 337 (1995).
17. Perrichon, V., Laachir, A., Abouarnadasse, S., Touret, O., and Blanchard, G., *Appl. Catal. A* **129**, 69 (1995).
18. Kępiński, L., and Wołcyrz, M., *J. Solid State Chem*. **131**, 121 (1997).